Aerosol Assisted Chemical Vapour Deposition of Zinc Oxide from Single Source *β*-Iminoesterate Precursors

Joe A. Manzi,[a] Caroline E. Knapp,[a] Ivan P. Parkin[a] and Claire J. Carmalt[a]*

[a]*Materials Chemistry Centre, Department of Chemistry, University College London, London, 20 Gordon Street, London, WC1H 0AJ, UK.*

Corresponding author. Tel.: 44 207 6797528; fax: 44 207 6797463.
E-mail address: c.j.carmalt@ucl.ac.uk;
https://www.ucl.ac.uk/chemistry/staff/academic_pages/claire_carmalt

Keywords: zinc oxide, thin film, AACVD, single-source, *β*-iminoesterate, precursor development

Single source zinc *β*-iminoesterate precursors have been used for the first time in the aerosol assisted chemical vapour deposition (AACVD) of ZnO thin films. Depositions at 450 °C on silica-coated glass substrates produced strongly adherent films with excellent coverage of the substrate. The zinc *β*-iminoesterates $[Zn(L_1)_2]$ (**1**) and $[Zn(L_2)_2]$ (**2**) were synthesised from the reaction between $ZnEt_2$ and 2 equivalents of a synthesised *β*-iminoester ligand $CH_3C(NHCH(CH_3)_2)CHC(O)OCH_2CH_3$ (**L_1**) and $CH_3C(NHCH_3)CHC(O)OCH_2CH_3$ (**L_2**). The synthesized complexes were isolated and characterized by ^1H and ^{13}C NMR spectroscopy, mass spectroscopy and thermal gravitational analysis (TGA). The structures of the compounds were determined by single crystal X-ray diffraction. The ZnO films deposited from (**1**) and (**2**) were analyzed by glancing-angle X-ray powder diffraction (XRD), scanning electron microscopy (SEM), X-ray photoelectron spectroscopy (XPS) and their optical properties determined by UV/Vis/NIR transmission spectroscopy. These results reveal that the organic ligand attached to the N moiety of the zinc complex has a significant effect on the level of carbon incorporated into the deposited thin film. Upon annealing, highly transparent hexagonal wurtzite ZnO thin films were produced.

Introduction

Zinc Oxide (ZnO) is a II-VI semiconductor material with a wide band gap of 3.37 eV and a large excitation binding energy of 60 meV.[1] The use of ZnO in a number technological applications has been the driving force for both commercial and academic researchers in the field. ZnO based nanosystems which utilise the materials semiconductor photoactivity for photocatalytic oxidation and photoinduced superhydrophilicity have found notable use for self-cleaning and anti-fogging applications.[2,3,4,5] In the form of thin films, ZnO has been utilised for its optoelectronic properties in organic electronics,[6] solar cells,[7] invisible and flexible electronics[8] as well as for applications outside of optoelectronics including as gas sensors.[9]

ZnO thin films have been deposited *via* a number of routes including solution based methods such as sol-gel[10] and physical vapour deposition methods such as thermal evaporation[11] and sputtering.[12] Chemical vapour deposition (CVD), a technique which has been extensively adapted, is also widely used in a number of its variations including metal organic MO(CVD),[13] low pressure LP(CVD),[14] combustion C(CVD)[15] and aerosol assisted AA(CVD).[16,17] CVD is an industrially favoured technique for its large area coverage and ability to offer adherent, reproducible films at low cost.[18] AACVD in particular offers a number of advantages including removing volatility requirements for precursors, a high deposition rate and a simpler, more flexible deposition method.[19,20]

The most widely used CVD precursor for ZnO films is diethylzinc, which undergoes an *in-situ* reaction with an additional oxygen source to form ZnO thin films.[21,22,23] However, its highly pyrophoric nature and reactivity can be problematic with the occurrence of undesired pre-reactions and reaction times which are often too fast for application. An alternative to this type of 'dual source' approach is the synthesis of single source precursors in which the precursor complex contains a preformed Zn–O bond. Advantages of single source precursors include eliminating the need for precursor mixing, fewer opportunities for pre-reaction, reproducibility and greater stoichiometric control.[24] Precursors for ZnO films include commercial compounds such as zinc acetate,[25] zinc acetylacetonate[26] as well as synthesised compounds such as alkyl zinc alkoxides.[27] One class of compounds that have received relatively limited investigations are zinc *β*-ketoiminate/iminoesterates. These compounds offer significant potential given their successful application as CVD precursors for main group and transition metal oxide thin films including Ga_2O_3,[28] MgO[29] and TiO_2.[30] Advantages of these compounds include their versatility in which their thermal and physical properties can be adapted though the alteration of groups on either the back bone of the attached ligand

or on the nitrogen moiety. Matthews *et al.*[31] successfully employed zinc *β*-ketoiminate and zinc *β*-iminoesterate complexes as single source precursors in the MOCVD of ZnO thin films. Further MOCVD depositions using zinc *β*-ketoiminates both as single source precursors[32] and with an additional oxygen source in the form of O_2 as a reactant gas[33,34] have also been carried out. In this study we report the synthesis and characterisation of the known zinc *β*-iminoesterate [Zn(OC(OCH$_2$CH$_3$)CHC(CH$_3$)N(CH(CH$_3$)$_2$)$_2$] [Zn(L$_1$)$_2$] (**1**) and the novel zinc *β*-iminoesterate [Zn(OC(OCH$_2$CH$_3$)CHC(CH$_3$)N(CH$_3$))$_2$] [Zn(L$_2$)$_2$] (**2**). Further to existing literature, we expand their use to the AACVD system as single source precursors for the deposition of ZnO thin films. We illustrate the significant effect the identity of the organic ligand attached to the N moiety of the precursor can have on the composition of the deposited thin films.

Results and Discussion

Zinc Complex Synthesis and Precursor Studies

β-iminoester ligands CH$_3$C(NHCH(CH$_3$)$_2$)CHC(O)OCH$_2$CH$_3$ (**L$_1$**) and CH$_3$C(NHCH$_3$)CHC(O)OCH$_2$CH$_3$ (**L$_2$**) were synthesized in a condensation reaction between ethyl acetoacetate and isopropylamine and methylamine respectively. An adapted literature procedure[35] employing K-10 montmorillonite as a catalyst was followed, as shown in Scheme 1. Its low cost, a simpler set-up and environmental gains are all advantages cited for the use of K-10 montmorillonite, which has been reviewed by Kumar *et al.*[36] Complete reaction was confirmed by ^{1}H and ^{13}C NMR and (**L$_1$**) and (**L$_2$**) were both isolated as pale yellow liquids in good yields of 87 and 80% respectively.

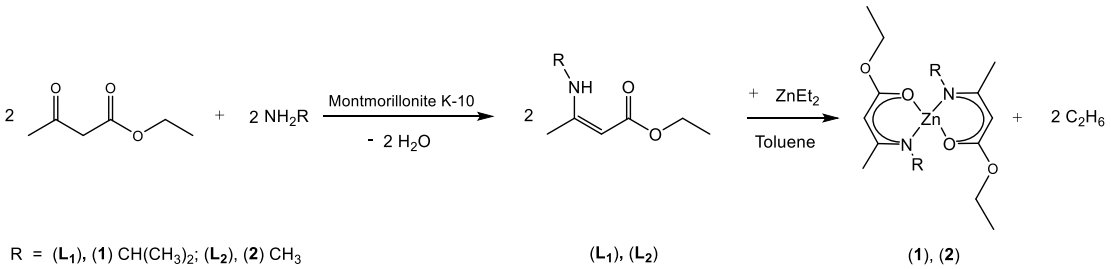

Scheme 1. The synthesis of *β*-iminoester ligands (**L$_1$**) and (**L$_2$**) and zinc *β*-iminoesterate complexes [Zn(L$_1$)$_2$] (**1**) and [Zn(L$_2$)$_2$] (**2**).

Zinc *β*-iminoesterate complexes [Zn(L_1)$_2$] (**1**) and [Zn(L_2)$_2$] (**2**) were synthesised in the reaction of 2 equivalents of (**L_1**) and (**L_2**) with $ZnEt_2$ respectively, as shown in Scheme 1. The ligand was added to a solution of diethylzinc in toluene at -78 °C, stirred and warmed to room temperature, during which time, ethane gas was observed to evolve. The zinc complexes [Zn(L_1)$_2$] (**1**) and [Zn(L_2)$_2$] (**2**) crystallised out of concentrated toluene solutions held at -18 °C as yellow tinted crystals in good yields of 85% and 72% respectively. The synthesis of (**1**) and (**2**) was confirmed by ^{1}H and ^{13}C NMR and mass spectroscopy, with the presence of the expected isotopic patterns and molecular ion peaks.

Single crystal X-ray diffraction structures of (**1**) and (**2**) were determined. The crystal structure of (**1**) has been previously reported by Matthews *et al*.[31] and is in good agreement with the data collected. The novel crystal structure of (**2**) is shown in Figure 1 with selected bond distances and angles given in Table 1 and the determined crystal data given in Table 2. [Zn(L_2)$_2$] (**2**) crystallises in the monoclinic space group $P2_{1/c}$ and is monomeric in the solid state. Two orthogonal iminoesterate ligands bond to a central, four coordinate zinc atom, which, as in (**1**), adopts a distorted tetrahedral geometry. There is significant deviation from the expected internal angle for a tetrahedral complex of 109.5° in both (**1**) and (**2**) due to the chelating nature of the ligand. The zinc centre in (**2**) has bond angles from 96.17 to 131.35°, similar to the 96.64 to 129.30° reported for (**1**).[31] These angles are as expected for compounds of this type and results from the inflexibility of the ligand and the relatively small bite angle resulting from the (RNC(CH_3)CHC(OCH_2CH_3)O) chain. The bond angles observed around the central Zn atom in (**2**) deviate from those observed in (**1**), most notably, the O(1)-Zn(1)-O(2) bond angle in (**2**) measures 122.56° compared to 110.97° in (**1**).[31] This is caused by the need to compensate for the reduced N(1)-Zn(1)-O(2) and N(2)-Zn(1)-O(1) bonds in (**2**) of 106.61 and 106.58° respectively (c.f. 111.77 and 110.29 for (**1**))[31] as a result of the reduced steric bulk of the methyl group on the N moiety in (**2**) compared to the isopropyl group on the N moiety in (**1**). The Zn-O and Zn-N bond lengths surrounding the zinc centre in both (**1**) and (**2**) are as expected for this type of compound and are typical of Zn-O and Zn-N bonds. As expected, the length of the C-N and C-O bonds within the delocalised system of (**2**) (1.318 Å for C(2)-N(1) and 1.266 Å for C(4)-O(1)) are shorter than the C-N and C-O bonds outside of the delocalised system (1.470 Å for C(7)-N(1) and 1.442 Å for C(5)-O(3)).

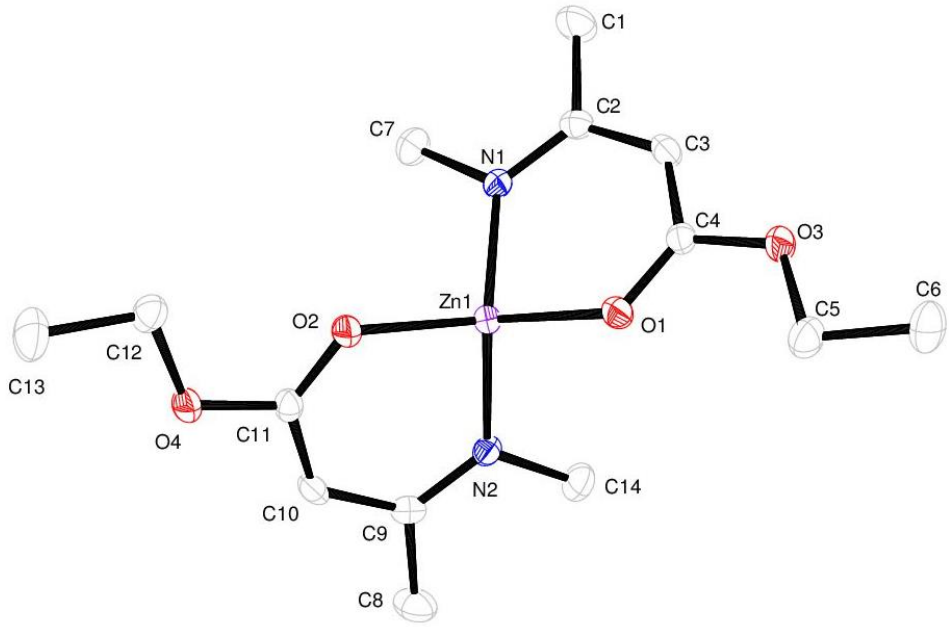

Figure 1: X-ray crystal structure of $[Zn(L_2)_2]$ (**2**)

Table 1: Selected bond distances (Å) and bond angles (°) for $[Zn(L_2)_2]$ (**2**)

Complex:	$[Zn(L_2)_2]$ (**2**)
Bond Lengths (Å)	
O(1)-Zn(1)	1.9815(14)
O(2)-Zn(1)	1.9726(13)
N(1)-Zn(1)	1.9583(19)
N(2)-Zn(1)	1.9552(18)
Bond Angles (°)	
O(1)-Zn(1)-O(2)	122.56(6)
O(1)-Zn(1)-N(1)	96.17(7)
O(1)-Zn(1)-N(2)	106.58(7)
O(2)-Zn(1)-N(1)	106.61(7)
O(2)-Zn(1)-N(2)	96.49(6)
N(1)-Zn(1)-N(2)	131.35(7)

Table 2: Crystal Data for $[Zn(L_2)_2]$ (**2**)

Complex:	$[Zn(L_2)_2]$ (**2**)

Formula	$[Zn(MeCN(Me)CHC(OEt)O)_2]$
Formula weight	349.75
Crystal system	Monoclinic
Space group	$P2_{1/c}$
a/Å	6.8111(4)
b/Å	20.8570(11)
c/Å	12.0757(7)
α/°	90
β/°	101.593(6)
γ/°	90
Volume /$Å^3$	1680.46(16)
$\rho_{calc}g/cm^3$	1.3823
Final R indexes [I>=2σ (I)]	R_1 = 0.0363, wR_2 = 0.0664

Thermal Gravimetric Analysis

Thermal gravimetric analysis (TGA) and differential scanning calorimetry (DSC) were performed between room temperature and 500 °C as shown in Figure 2. For both (**1**) and (**2**) a clean, one step decomposition is observed, an ideal feature for CVD precursors to exhibit. The decomposition of (**1**) is seen to begin at 140 °C with significant mass loss observed between 200 and 250 °C. A slight mass loss of 1.5% between 85 and 115 °C results from residual toluene, which also accounts for the small initial peak observed in the DSC.

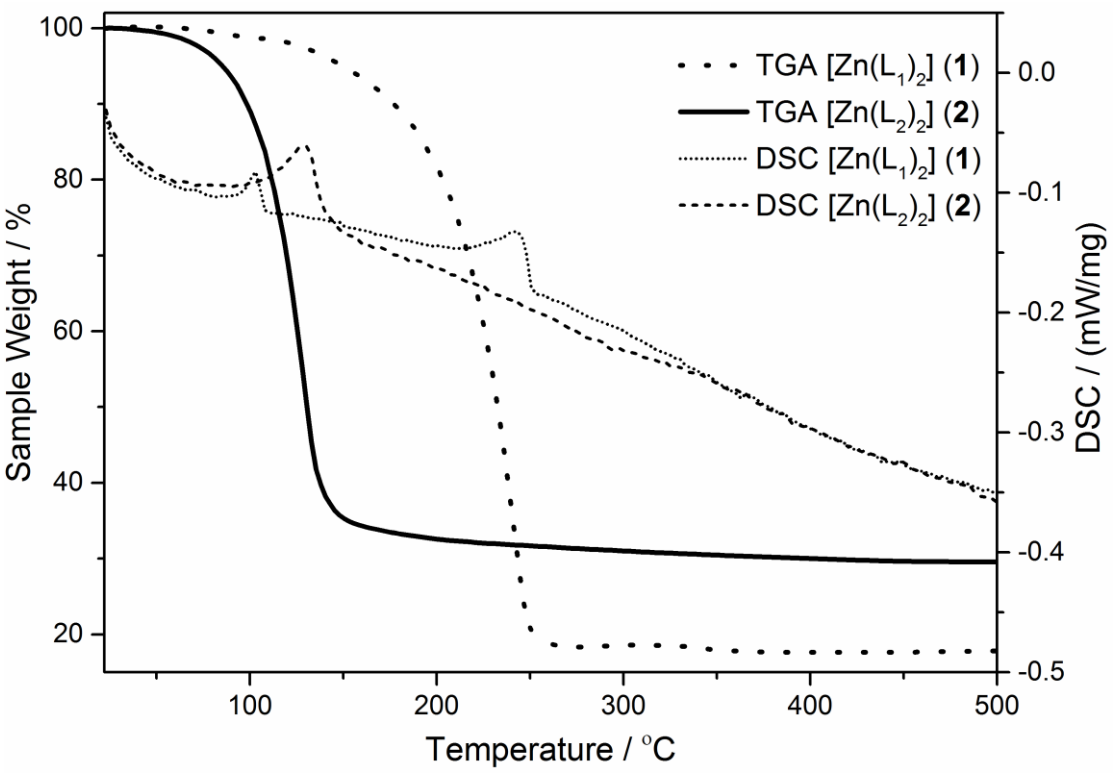

Figure 2. Thermal gravimetric analysis and differential scanning calorimetry profiles observed for zinc complex $[Zn(L_1)_2]$ (**1**) and $[Zn(L_2)_2]$ (**2**).

The observed residual mass of (**1**) at 500 °C is 19.8% which matches closely to the calculated residual mass of 20.1% for ZnO. This is suggestive of a clean decomposition of (**1**) to zinc oxide. Complex (**2**) is observed to be more volatile at a lower temperature, with significant mass loss observed between 100 – 140 °C. The observed residual mass for (**2**) is 29.6% which is larger than the expected residual mass for ZnO for the compound of 23.2%. This could be suggestive of incomplete decomposition of (**2**) and the potential for contamination of deposited films by impurities.

AACVD

Zinc *β*-iminoesterate complexes $[Zn(L_1)_2]$ (**1**) and $[Zn(L_2)_2]$ (**2**) were both successfully employed as precursors in the AACVD of ZnO thin films on silica coated float glass as shown in Scheme 2. Initial studies were conducted involving varying substrate temperature and N_2 flow rates between 350 and 550 ˚C and 0.8 and 2 $Lmin^{-1}$ respectively. The optimum deposition conditions were found to be 450 °C and 1 $Lmin^{-1}$. Depositions were carried out using dry toluene as a solvent and also in dry dioxane as a comparison. Excellent solubility

was observed for both (**1**) and (**2**) in these solvents. The as-deposited films from (**1**) had a light brown tint whereas the films from (**2**) appeared noticeably darker, suggestive of greater carbon contamination. Upon annealing the brown colour was removed from all samples resulting in highly transparent thin films with transparency greater than 90% in the visible light region.

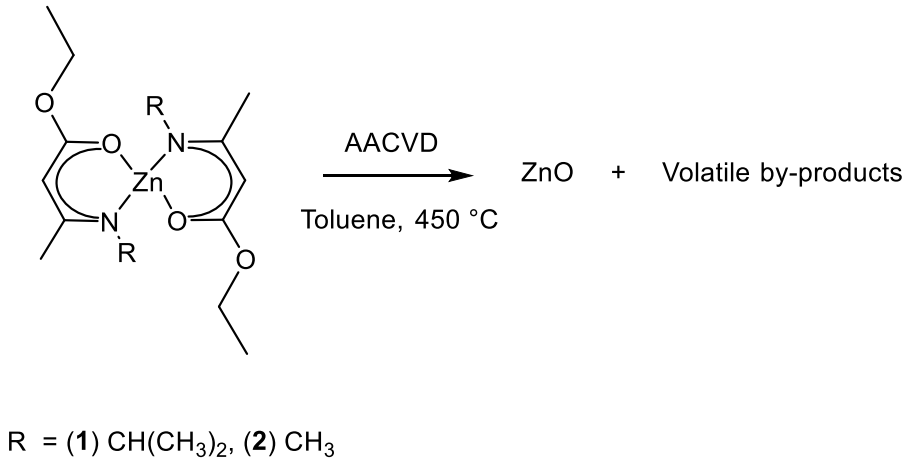

Scheme 2. The AACVD of ZnO thin films from *β*-iminoesterate precursors [Zn(L_1)$_2$] (**1**) and [Zn(L_2)$_2$] (**2**).

The films exhibited excellent coverage of the entire substrate and were strongly adherent, passing the Scotch© tape test and only being removed upon intense scratching with a steel scalpel. The deposited films were insoluble in common organic solvents (acetone, toluene and 2-propanol) but dissolved in nitric acid. The as-deposited films were not electrically conductive but upon annealing became slightly conductive, with a resistance of 5 MΩ for films deposited from (**1**) and 40 MΩ for films deposited from (**2**). These values are as expected for undoped zinc oxide, which is typically highly resistive[37] and for significant conductivity a dopant source would be required. Film thickness was determined using a Filmetrics F20 thin film measurement system. As-deposited films from [Zn(L_2)$_2$] (**2**) were found to be around 550 nm thick compared to the 350 nm measured for films as-deposited from [Zn(L_1)$_2$] (**1**). Upon annealing, films from both (**1**) and (**2**) were found to be between 280 and 300 nm in thickness. These figures are explained by XPS analysis which shows incorporation of carbon and nitrogen in films from (**2**) which is subsequently removed upon annealing. The films were characterized using X-ray photoelectron spectroscopy (XPS), glancing-angle X-ray powder diffraction (XRD), scanning electron microscopy (SEM) and their optical properties were studied using UV/Vis/NIR transmission spectroscopy.

X-ray photoelectron spectroscopy

XPS of the annealed thin films deposited from zinc complexes $[Zn(L_1)_2]$ (**1**) and $[Zn(L_2)_2]$ (**2**) confirm the presence of Zn and O. The Zn 2p peaks were fitted by a Gaussian/Lorentzian product distribution. As expected, characteristic peaks for the Zn $2p_{1/2}$ and $2p_{3/2}$ states appear at 1045.18 and 1022.18 eV binding energy respectively, with an intensity ratio of 1:2 and an energy gap of 23.0 eV as shown in Figure 3.[38] The O 1s peak can be fitted by a Gaussian distribution centred at 531.4 eV as would be expected.

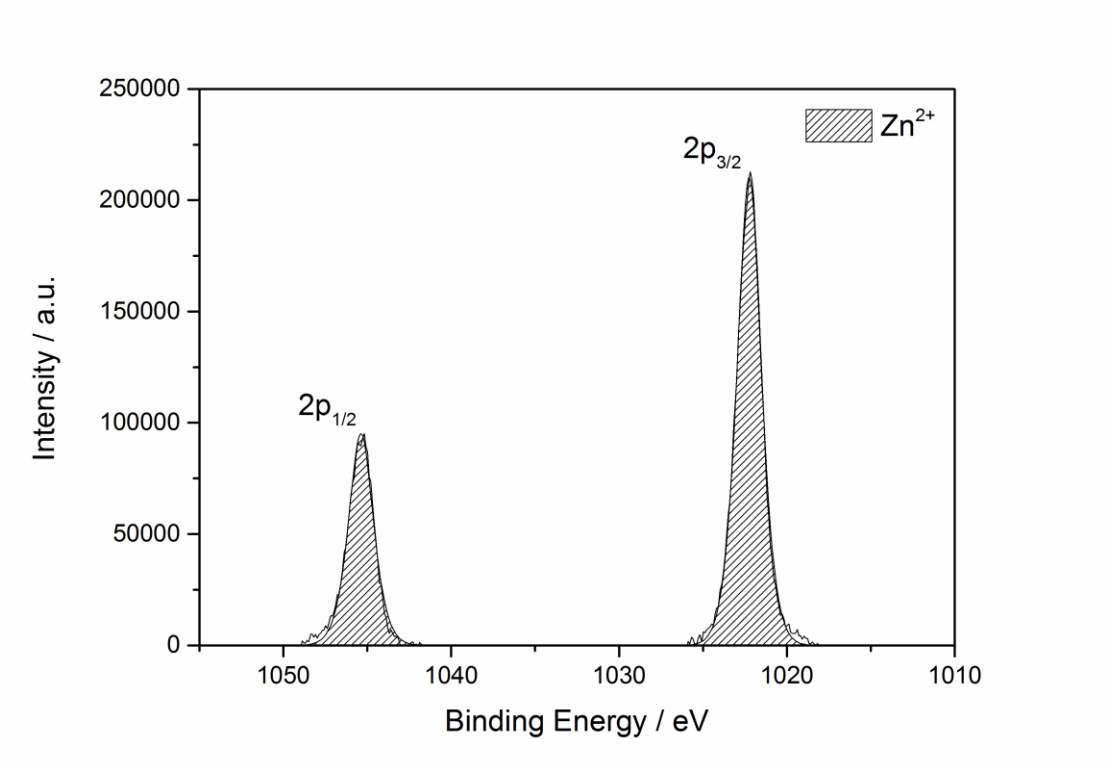

Figure 3. XPS of Zn 2p from a ZnO thin film deposited from $[Zn(L_1)_2]$ (**1**) at 450 °C by AACVD in toluene.

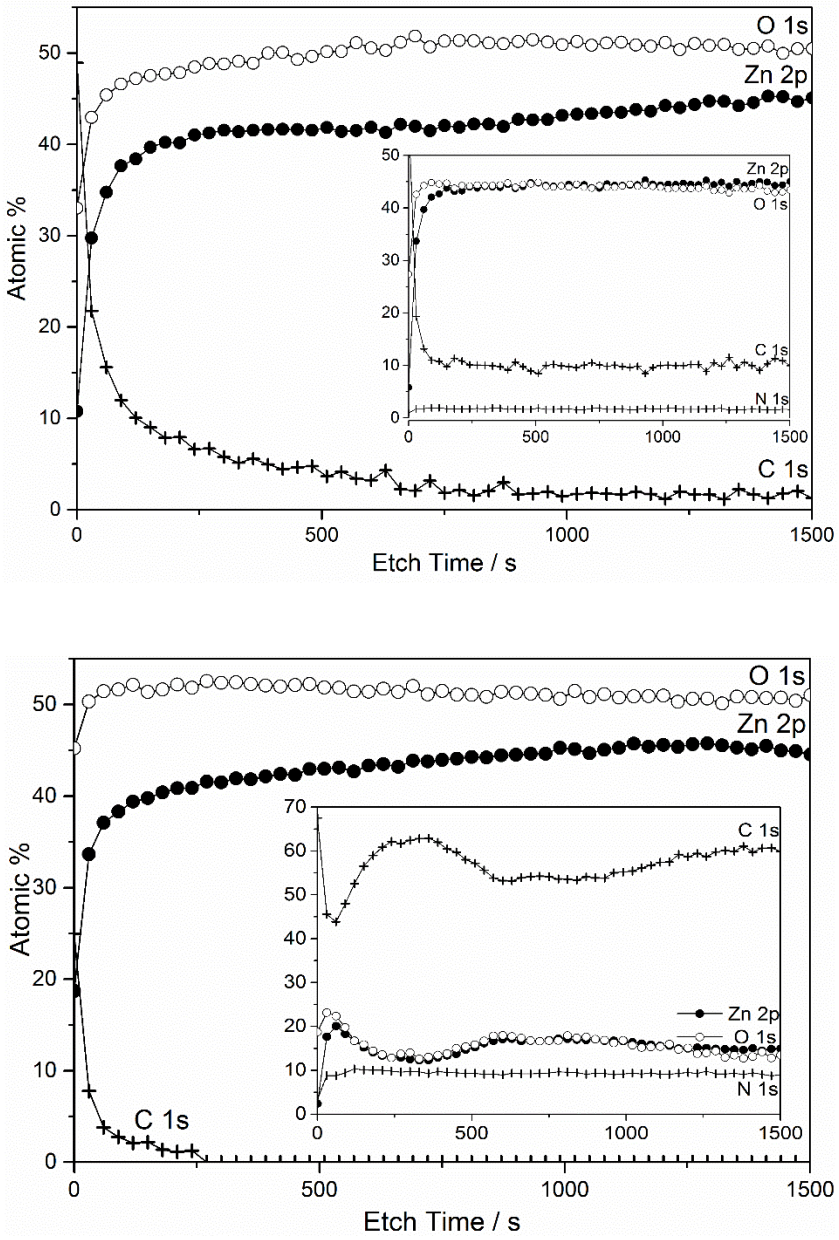

Figure 4. XPS depth profile for annealed films deposited from zinc complex $[Zn(L_1)_2]$ (**1**) (upper) and zinc complex $[Zn(L_2)_2]$ (**2**) (lower) in toluene. Inset: XPS depth profile for the respective as-deposited films.

The as-deposited films were found to contain carbon throughout the entirety of the film. Average carbon content in the as-deposited films from $[Zn(L_1)_2]$ (**1**) in toluene was found to be 9.7 at.% as seen in Figure 4 (upper, inset). The carbon content was also found to be related to the solvent used. When dioxane was used as a solvent the carbon content averaged 10.2 at.% but decreased when hexane was used to 5.7 at.%. These figures are in a similar range to

the 8.7 at.% reported by Matthews *et al.*[31] for ZnO films deposited from (**1**) by AP-MOCVD. Upon annealing this falls to 3.1 at.% as can be seen in Figure 4 (upper), resulting in a $ZnO_{1.2}$ transparent thin film. For films deposited from $[Zn(L_2)_2]$ (**2**) in toluene the carbon content of the film was found to be 56.1 at.%, as shown in Figure 4 (lower, inset). There was also significant nitrogen content at 9.0 at.%, compared to less than 1 at.% in the thin film deposited from (**1**). This is suggestive of contamination from precursor molecules that have been unable to undergo complete decomposition. The large residual mass observed in the TGA of (**2**) supports this theory. It is postulated that due to the bulkier organic ligand group on the N moiety in precursor (**1**) there are more facile decomposition routes, such as hydride elimination mechanisms accessible which are not available in precursor (**2**). This leads to the large difference of nitrogen and carbon content observed in the as-deposited film from (**1**) and (**2**). Comparative carbon content in ZnO films deposited from single source MOCVD of zinc *β*-ketoiminate range from approximately 10 at.%[32] up to 26.2 at.%.[31] The carbon content figures obtained illustrate further the significant effect the identity of the organic ligand attached to the N on the zinc complex has on the level of carbon content in the deposited thin film. Upon annealing, the carbon content of the film deposited from (**2**) fell dramatically to 0.6 at.%, as shown in Figure 4 (lower) resulting in a transparent $ZnO_{1.2}$ thin film.

X-ray diffraction

Glancing-angle X-ray diffraction (XRD) patterns of the as-deposited and annealed films deposited from (**1**) and (**2**) in toluene are shown in Figure 5. Peaks observed in the pattern for the annealed films from both (**1**) and (**2**) confirm the formation of the hexagonal wurtzite crystal structure of ZnO. NOTE TO EDITOR: TEXT REMOVED HERE. The amorphous nature of carbon also explains why no peaks were observed in the pattern for the as-deposited film from zinc complex (**2**). Similar XRD patterns are observed when dioxane is used as the solvent.

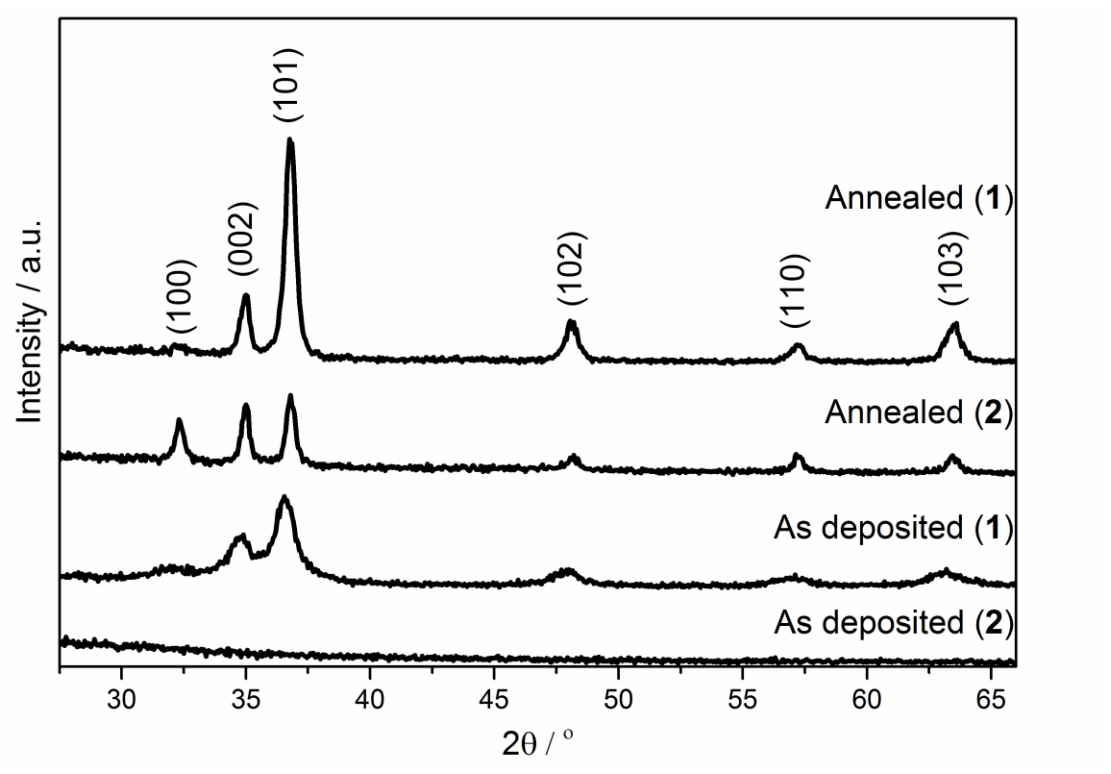

Figure 5. XRD patterns obtained from as-deposited and annealed films deposited from zinc complex $[Zn(L_1)_2]$ (**1**) and $[Zn(L_2)_2]$ (**2**) at 450 °C by AACVD in toluene.

Scanning electron microscopy

Scanning electron microscopy (SEM) was used to determine surface morphology of the as-deposited and annealed films as shown in Figure 6. The as-deposited films (Figure 6, A and C) were found to be dense and continuous ZnO coatings.

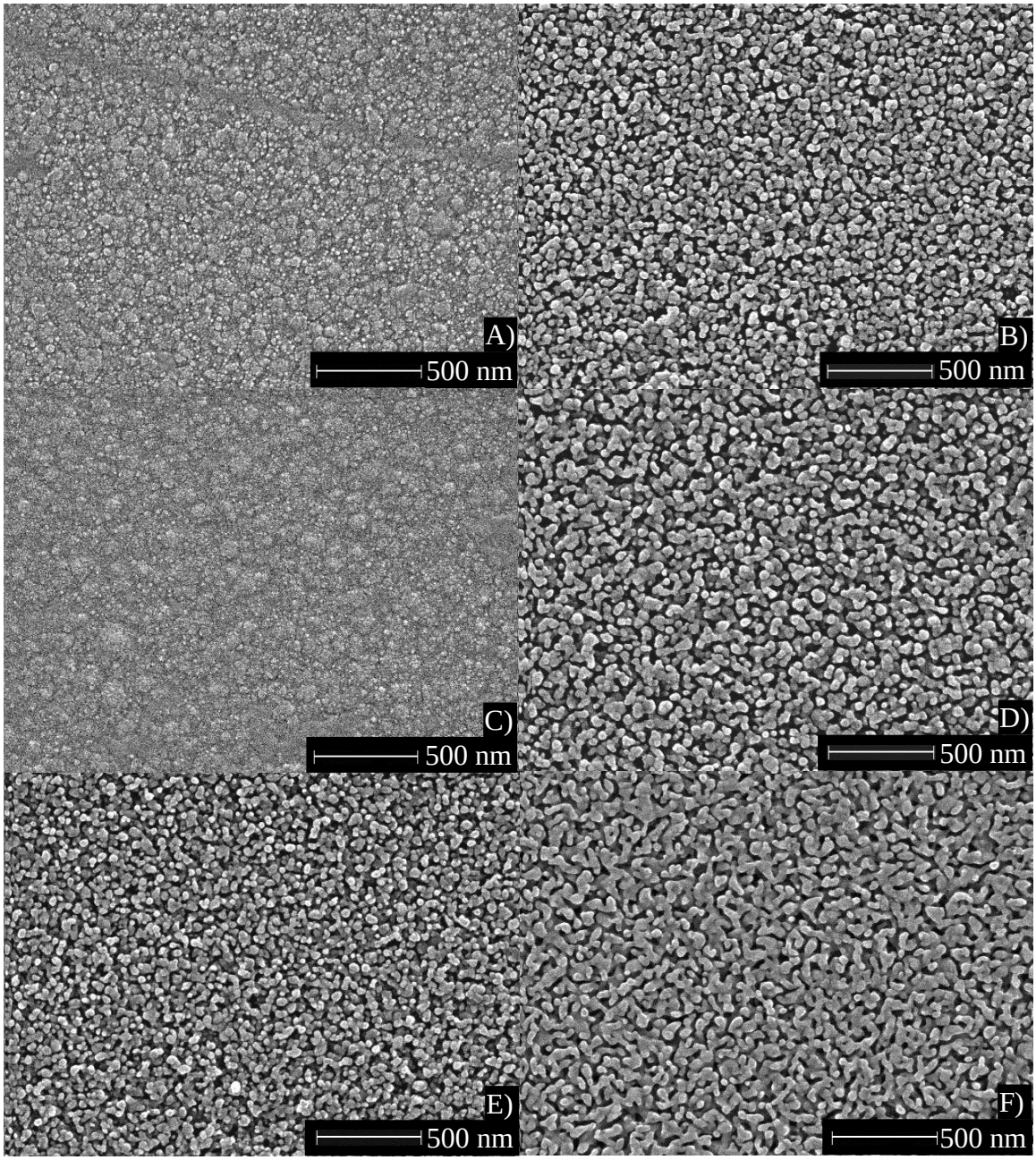

Figure 6. High magnification (*x*50,000) plane view SEM images of thin films deposited from $[Zn(L_1)_2]$ (**1**) (A - D) and $[Zn(L_2)_2]$ (**2**) (E and F). As-deposited films are shown in A and C with annealed films shown in B and D-F. Films A, B and E were deposited using toluene as a solvent and films C, D and F using dioxane.

Upon annealing (Figure 6, B and D – F) the structure of agglomerated particles becomes more evident and is indicative of a Volmer-Weber type island growth mechanism. This occurs when depositing particles have a stronger attraction to themselves as opposed to the underlying substrate. The microstructure observed also illustrates a significant presence of

grain boundaries in the films which is consummate with their low conductivity. The identity of the solvent was also found to have an influence on the structure of the films. A greater degree of agglomeration and increased size of particle clusters was observed when dioxane was used as a solvent (Figure 6, D and F) compared to when toluene was used (Figure 6, B and E). The particles in films deposited from (**2**) in dioxane (Figure 6, F) were also found to be more elongated as opposed to rounded in nature.

Optical properties

The transmission properties of the as-deposited and annealed films from $[Zn(L_1)_2]$ (**1**) and $[Zn(L_2)_2]$ (**2**) in toluene were studied using UV/Vis/NIR spectroscopy recorded between 300 and 1400 nm, as shown in Figure 7. As-deposited films from $[Zn(L_1)_2]$ (**1**) and $[Zn(L_2)_2]$ (**2**) had a visible light transmission of 74 and 41% respectively. The significantly lower transmission of the film deposited from (**2**) is again related to the high carbon content of the film, as shown by XPS measurements. Upon annealing, the average transmission of the films in the visible light region from (**1**) and (**2**) increases to 90%. These figures exceed the 80% value often quoted for a film to be described as highly transparent.[39]

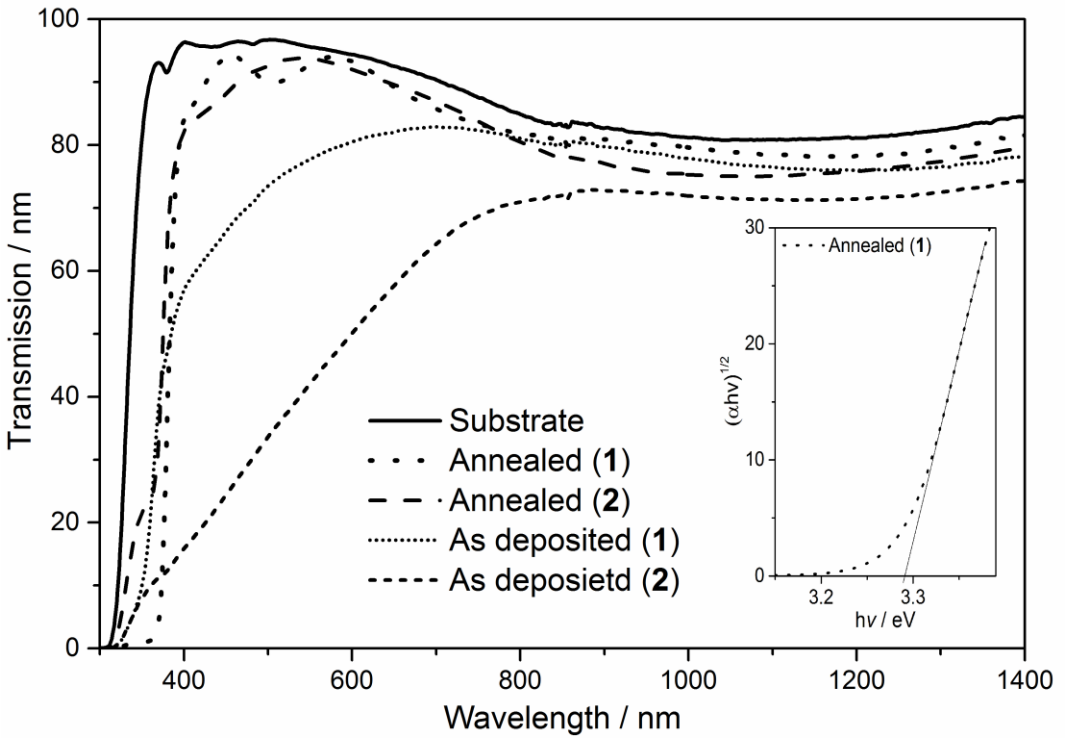

Figure 7. Transmission spectra observed for as-deposited and annealed thin films deposited from $[Zn(L_1)_2]$ (**1**) and $[Zn(L_2)_2]$ (**2**) in toluene at 450 °C by AACVD. Inset: Tauc plot for annealed film deposited from $[Zn(L_1)_2]$ (**1**) with fitting line.

The adsorption edge, shown by the sharp decrease in transmission of the annealed films, has been used to estimate the optical band gap using the Tauc relation.[40] Estimates are made from the intercept of the *hv* axis from a line of steepest gradient for the linear region of a $(ahv)^{1/2}$ *vs. hv* plot, as shown for the annealed film from (**1**) inset in Figure 7. The band gap of the annealed zinc oxide films was determined to be 3.3 eV for the film from (**1**) and 3.4 eV for the film from (**2**). These figures match well with the literature value of 3.37 eV.[1]

Conclusions

Two zinc complexes, the known zinc *β*-iminoesterate $[Zn(L_1)_2]$ (**1**) and the novel zinc *β*-iminoesterate $[Zn(L_2)_2]$ (**2**), where (**L_1**) is $CH_3C(NHCH(CH_3)_2)CHC(O)OCH_2CH_3$ and (**L_2**) is $CH_3C(NHCH_3)CHC(O)OCH_2CH_3$ were successfully synthesised, characterised and their structures determined by single crystal X-ray crystallography. The isolated complexes were used for the first time as AACVD precursors resulting in the deposition of ZnO thin films which were highly adherent and exhibited excellent coverage of the substrate. The identity of the organic ligand attached to the N moiety of the precursor was found to have a significant effect on the carbon content of the deposited film. A difference greater than 45 at.% was observed in the carbon content of the films deposited from $[Zn(L_1)_2]$ (**1**) and $[Zn(L_2)_2]$ (**2**). TGA was shown to be a useful technique for indicating the likelihood of potential contamination. Upon annealing, highly transparent ZnO thin films with the hexagonal wurtzite structure and transparency greater than 90% in the visible light region were yielded. Here, we have shown the ability of using a non-pyrophoric, stable zinc *β*-iminoesterates as precursors for the AACVD of ZnO thin films. Further studies are required to investigate in greater detail the connection between ligand identity and carbon content of deposited films and to investigate the addition of dopants to improve the conductivity.

Experimental

Synthesis

Caution: $ZnEt_2$ is a pyrophoric substance which may ignite spontaneously in air. Fumes produced during the CVD of zinc compounds can potentially be toxic and corrosive and all dispositions should be carried out in a fume hood.

All manipulations involving the formation of the zinc complexes were performed under a dry dinitrogen atmosphere using standard Schlenk line techniques or in a Mbraun glovebox. All solvents used were stored in alumina columns and dried with anhydrous engineering equipment such that water concentrations were below 10 ppm. Methylamine solution (2 M in tetrahydrofuran), isopropylamine, ethyl acetoacetate, diethylzinc solution (15 wt.% in toluene) and K-10 montmorillonite clay were obtained from Sigma Aldrich and used as supplied. ^{1}H and ^{13}C NMR spectra were obtained on a Bruker Avance III 600 cryo spectrometer and were recorded in $CDCl_3$. ^{1}H and ^{13}C chemical shifts are reported relative to $SiMe_4$ (δ 0.00). Mass spectroscopy was performed on a Thermo Finnigan MAT900 XP operating in EI and CI mode.

(**L_1**) and (**L_2**) were prepared using an modified literature procedure.[35] Experimental details are provided below.

$CH_3C(NHCH(CH_3)_2)CHC(O)OCH_2CH_3$ (**L_1**) Isopropylamine (150 mmol, 12.89 mL) was added dropwise to ethyl acetoacetate (75 mmol, 9.49 mL) dispersed over K-10 montmorillonite clay (40 g) in a 3-necked round-bottom flask fitted with an overhead mechanical stirrer. The reaction slurry initially gave out heat and was stirred at room temperature for 6 hours. The product was extracted by washing with dichloromethane (3 x 50 mL) and filtered. The solvent was removed *in vacuo* to yield a pale yellow liquid. Yield: 11.17 g, 87%. **^{1}H NMR δ/ppm ($CDCl_3$):** 1.18 (d, 6H, *J* = 6.4 Hz, $(C\underline{H}_3)_2$), 1.21 (t, 3H, *J* = 7.1 Hz, $C\underline{H}_3CH_2$), 1.91 (s, 3H, $C\underline{H}_3C$), 3.65 (m, 1H, $(CH_3)_2C\underline{H}$), 4.05 (q, 2H, *J* = 7.1 Hz, $CH_3C\underline{H}_2$), 4.36 (s, 1H, $C\underline{H}CO$), 8.47 (s (broad), 1H, $N\underline{H}$). **$^{13}C\{^{1}H\}$ NMR δ/ppm ($CDCl_3$):** 14.8 ($\underline{C}H_3CH_2$), 19.3 ($\underline{C}H_3C$), 24.2 ($(\underline{C}H_3)_2$), 44.5 ($\underline{C}H(CH_3)_2$), 58.3 ($CH_3\underline{C}H_2$), 81.8 ($\underline{C}HCO$), 160.9 (q) ($\underline{C}NH$), 170.7 (q) ($\underline{C}O$). **MS: m/z $[M+H]^{+\cdot}$:** 172.16.

$CH_3C(NHCH_3)CHC(O)OCH_2CH_3$ (**L_2**) Methylamine (150 mmol, 4.66 g) as a 33 wt.% solution in ethanol (18.67 mL) was added dropwise to ethyl acetoacetate (75 mmol, 9.49 mL) dispersed over K-10 montmorillonite clay (60 g) in a 3-necked round-bottom flask fitted with an overhead mechanical stirrer. The reaction slurry initially gave out heat and was stirred at room temperature for 6 hours. The product was extracted by washing with dichloromethane (3 x 50 mL) and filtered. The solvent was removed *in vacuo* to yield a pale yellow liquid. Yield: 8.58 g, 80%. **^{1}H NMR δ/ppm ($CDCl_3$):** 1.20 (t, 3H, *J* = 7.1 Hz, $C\underline{H}_3CH_2$), 1.87 (s, 3H, $C\underline{H}_3C$), 2.86 (d, 3H, *J* = 5.2 Hz, $C\underline{H}_3NH$), 4.04 (q, 2H, *J* = 7.1 Hz, $CH_3C\underline{H}_2$), 4.42 (s, 1H, $C\underline{H}CO$), 8.44, (s (broad), 1H, $N\underline{H}$). **$^{13}C\{^{1}H\}$ NMR δ/ppm ($CDCl_3$):** 14.7 ($\underline{C}H_3CH_2$), 19.3

(*C*H$_3$C), 29.6 (*C*H$_3$NH), 58.3 (CH$_3$*C*H$_2$), 81.9 (*C*HCO), 162.9 (q) (*C*NH), 170.7 (q) (*C*O). **MS: m/z [M+H]$^{+\cdot}$:** 144.10.

[Zn(L$_1$)$_2$] (**1**) was prepared using a modified literature procedure,[31] with experimental details provided below.

[Zn(OC(OCH$_2$CH$_3$)CHC(CH$_3$)N(CH(CH$_3$)$_2$)$_2$] [Zn(L$_1$)$_2$] (**1**) Diethylzinc (8.76 mmol, 1.08 g) as a 15 wt.% toluene solution (7.88 mL) was added to dry toluene (10 mL) at -78 °C. **L$_1$** (17.52 mmol, 3.00 g) was added dropwise to the diethylzinc solution. The resulting solution was brought to room temperature and stirred for 24 hours. Toluene (~15 mL) was partially removed *in vacuo* and the remaining solution was left at -18 °C for 48 hours. The product crystallised out as yellow tinted crystals. Yield: 3.01 g, 85%. **^{1}H NMR δ/ppm (CDCl$_3$):** 1.09 (d, 6H, *J* = 5.4 Hz, (C*H*$_3$)$_2$CH), 1.10 (d, 6H, *J* = 5.4 Hz, (C*H*$_3$)$_2$CH), 1.23 (t, 6H, *J* = 7.1 Hz, C*H*$_3$CH$_2$), 1.98 (s, 6H, C*H*$_3$C), 3.85 (m, 2H, *J* = 6.4 Hz, (CH$_3$)$_2$C*H*), 4.08 (q, 4H, *J* = 7.1 Hz, CH$_3$C*H*$_2$), 4.30 (s, 2H, C*H*CO). **^{13}C{^{1}H} NMR δ/ppm (CDCl$_3$):** 15.00 (*C*H$_3$CH$_2$), 22.4 (*C*H$_3$C), 24.8 ((*C*H$_3$)$_2$CH), 49.8 ((CH$_3$)$_2$*C*H), 59.2 (CH$_3$*C*H$_2$), 78.0 (*C*HCO), 170.5 (q) (*C*N), 171.0 (q) (*C*O). **MS: m/z [M]$^{+\cdot}$:** 405.52.

[Zn(OC(OCH$_2$CH$_3$)CHC(CH$_3$)N(CH$_3$))$_2$] [Zn(L$_2$)$_2$] (**2**) Diethylzinc (10.47 mmol, 1.29 g) as a 15 wt.% toluene solution (9.43 mL) was added to dry toluene (10 mL) at -78 °C. **L$_2$** (20.95 mmol, 3.00 g) was added dropwise to the diethylzinc solution. The resulting solution was brought to room temperature and stirred for 24 hours. Toluene (~15mL) was partially removed *in vacuo* and the remaining solution was left at -18 °C for 48 hours. The product crystallised out as pale yellow tinted crystals. Yield: 2.63 g, 72%. **^{1}H NMR δ/ppm (CDCl$_3$):** 1.25 (t, 6H, *J* = 7.1 Hz, C*H*$_3$CH$_2$), 1.95 (s, 6H, C*H*$_3$C), 3.01 (s, 6H, C*H*$_3$N), 4.09 (q, 4H, *J* = 7.1 Hz, CH$_3$C*H*$_2$), 4.36 (s, 2H, *J* = 7.1 Hz, C*H*CO). **^{13}C{^{1}H} NMR δ/ppm (CDCl$_3$):** 14.9 (*C*H$_3$CH$_2$), 21.7 (*C*H$_3$C), 37.7 (*C*H$_3$N), 59.4 (CH$_3$*C*H$_2$), 77.8 (*C*HCO), 171.9 (q) (*C*N), 174.5 (q) (*C*O). **MS: m/z [M]$^{+\cdot}$:** 349.09.

AACVD

General procedures

Nitrogen (99.99%) was obtained from BOC and used as supplied. Films were deposited onto Pilkington NSG float-glass substrates (145 mm *x* 45 mm *x* 4 mm) with a 25 nm barrier layer

of crystalline SiO_2. A second glass plate was held 6 mm above the glass substrate in order to quash any air turbulence and ensure a laminar gas flow. The glass substrate was cleaned prior to deposition using isopropyl alcohol and acetone. The precursors were dissolved in a suitable solvent which had been stored in an alumina column and dried with anhydrous engineering equipment such that the water concentration was below 10 ppm. A Liquifog® piezo ultrasonic atomizer was used to create an aerosol mist from the precursor solution which was carried from a glass AACVD bubbler, though a brass baffle and into the cold-walled, horizontal-bed CVD reactor using a N_2 carrier gas at a flow rate of 1 $Lmin^{-1}$. The substrate was heated to 450 °C on a graphite block containing a Whatman cartridge heater, the temperature of which was controlled and monitored using a Platinum-Rhodium thermocouple. After deposition, the glass substrates were allowed to cool under a flow of nitrogen to below 100 °C before being removed. Coated substrates were handled and stored in air. All depositions were carried out in a fumehood.

AACVD from $[Zn(L_1)_2]$ (1) and $[Zn(L_2)_2]$ (2)

0.5 g of complex (**1**) was dissolved in dry toluene (20 mL) inside a glass bubbler under N_2 and stirred for 10 minutes. Once the arerosol was created the deposition took 30 minutes to complete. Depositions from precursor (**1**) were also carried out in dry dioxane and dry hexane. Depositions from precursor (**2**) (0.5 g) were carried out under the same conditions in dry toluene and dry dioxane.

Analysis Methods

Thermal gravimetric analysis (TGA) and differential scanning calorimetry (DSC) were performed using a Netzsch STA 449 C Jupiter Thermo-microbalance between room temperature and 500 °C under helium in an open aluminum pan. Single crystal X-ray diffraction datasets of $[Zn(L_1)_2]$ (**1**) and $[Zn(L_2)_2]$ (**2**) were collected on a SuperNova (dual source) Atlas diffractometer. Single crystals of (**1**) and (**2**) were selected, mounted on a nylon loop and kept at 150 K during data collection. The dataset for zinc *β*-iminoesterate (**1**) was collected using monochromated Cu Kα radiation (λ = 1.54184 Å) with monochromated Mo Kα (λ = 0.71073 Å) used for the collection of the dataset for zinc *β*-iminoesterate (**2**). Olex2[41] was used to solve the two structures with the Superflip[42] structure solution programme using charge flipping. The structure of (**1**) was refined using the SHELX[43] refinement package employing Least Squares minimisation whilst the structure of (**2**) was refined using the

olex2.refine[44] refinement package using Gauss-Newton minimisation. X-ray diffraction (XRD) patterns were recorded using a Bruker D8 Discover X-ray diffractometer using monochromatic Cu $K\alpha_1$ and Cu $K\alpha_2$ radiation of wavelengths 1.54056 and 1.54439 Å respectively, emitted in an intensity ratio of 2:1 with a voltage of 40 kV and a current of 40 mA. Compound **2** was submitted to the CCDC; no. 1052924. Scanning electron microscopy (SEM) was performed using a Philips XL30 FEG operating in plan mode with an electron beam accelerating energy of 30 kV and an instrument magnification of 50,000*x*. Film thickness was estimated using a Filmetrics F20 thin film measurement system. X-ray photoelectron spectroscopy (XPS) surface and depth profiling was performed using a Thermo Scientific K-Alpha XPS system using monochromatic Al Kα radiation at 1486.6 eV X-ray source. Etching was achieved using an Ar ion etch beam at 1 KeV with a current of 1.51 μA. CasaXPS software was used to analyses the data with binding energies referenced to an adventitious C 1s peak at 284.8 eV. UV/Vis/NIR transmission spectra were recorded using a PerkinElmer Lambda 950 spectrometer in the range of 300 – 1400 nm with an air background.

Supporting Information (see footnote on the first page of this article): ^{1}H NMR spectroscopic data for compound **2** is provided.

Acknowledgements

The EPSRC are thanked for studentship funding (JAM) through the Molecular Modelling and Materials Science Doctoral Training Centre (grant EP/G036675) and the grants EP/K001515 and EP/L017709. NSG Pilkington are thanked for SEM and XPS analysis and funding (JAM). Deborah Raisbeck (NSG Pilkington) is thanked for assistance provided.

References

[1] L. Wang and N. C. Giles, *J. Appl. Phys.*, **2003**, *94*, 973.

[2] D. Barreca, A. Gasparotto, C. Maccato, E. Tondello, U. L. Štangar and S. R. Patil, *Surf. Coat. Technol.*, **2009**, *203*, 2041–2045.

[3] L. Armelao, D. Barreca, G. Bottaro, A. Gasparotto, D. Leonarduzzi, C. Maragno, E. Tondello and C. Sada, *J. Vac. Sci. Technol. Vac. Surf. Films*, **2006**, *24*, 1941.

[4] D. Barreca, A. P. Ferrucci, A. Gasparotto, C. Maccato, C. Maragno and E. Tondello, *Chem. Vap. Depos.*, **2007**, ***13***, 618–625.

[5] D. Bekermann, A. Gasparotto, D. Barreca, A. Devi, R. A. Fischer, M. Kete, U. Lavrenčič Štangar, O. I. Lebedev, C. Maccato, E. Tondello and G. Van Tendeloo, *ChemPhysChem*, **2010**, *11*, 2337–2340.

[6] G. Luka, M. Godlewski, E. Guziewicz, P. Stakhira, V. Cherpak and D. Volynyuk, *Semicond. Sci. Technol.*, **2012**, *27*, 074006.

[7] Y. Sun, J. H. Seo, C. J. Takacs, J. Seifter and A. J. Heeger, *Adv. Mater.*, **2011**, *23*, 1679–1683.

[8] E. M. C. Fortunato, P. M. C. Barquinha, A. C. M. B. G. Pimentel, A. M. F. Gon**?**alves, A. J. S. Marques, L. M. N. Pereira and R. F. P. Martins, *Adv. Mater.*, **2005**, *17*, 590–594.

[9] M. A. Chougule, S. Sen and V. B. Patil, *Ceram. Int.*, **2012**, *38*, 2685–2692.

[10] L. Znaidi, *Mater. Sci. Eng. B*, **2010**, *174*, 18–30.

[11] O. Fouad, A. Ismail, Z. Zaki and R. Mohamed, *Appl. Catal. B Environ.*, **2006**, *62*, 144–149.

[12] R. Ondo-Ndong, F. Pascal-Delannoy, A. Boyer, A. Giani and A. Foucaran, *Mater. Sci. Eng. B*, **2003**, *97*, 68–73.

[13] A. Hongsingthong, I. Afdi Yunaz, S. Miyajima and M. Konagai, *Sol. Energy Mater. Sol. Cells*, **2011**, *95*, 171–174.

[14] S. Faÿ, U. Kroll, C. Bucher, E. Vallat-Sauvain and A. Shah, *Sol. Energy Mater. Sol. Cells*, **2005**, *86*, 385–397.

[15] I. Zunke, A. Heft, P. Schäfer, F. Haidu, D. Lehmann, B. Grünler, A. Schimanski and D. R. T. Zahn, *Thin Solid Films*, **2013**, *532*, 50–55.

[16] D. S. Bhachu, G. Sankar and I. P. Parkin, *Chem. Mater.*, **2012**, *24*, 4704–4710.

[17] M. R. Waugh, G. Hyett and I. P. Parkin, *Chem. Vap. Depos.*, **2008**, *14*, 366–372.

[18] L. G. Bloor, J. Manzi, R. Binions, I. P. Parkin, D. Pugh, A. Afonja, C. S. Blackman, S. Sathasivam and C. J. Carmalt, *Chem. Mater.*, **2012**, *24*, 2864–2871.

[19] X. Hou and K.-L. Choy, *Chem. Vap. Depos.*, **2006**, *12*, 583–596.

[20] P. Marchand, I. A. Hassan, I. P. Parkin and C. J. Carmalt, *Dalton Trans.*, **2013**, *42*, 9406.

[21] G. Walters and I. P. Parkin, *Appl. Surf. Sci.*, **2009**, *255*, 6555–6560.

[22] Z. Shi, S. Zhang, B. Wu, X. Cai, J. Zhang, W. Yin, H. Wang, J. Wang, X. Xia, X. Dong, B. Zhang and G. Du, *Appl. Surf. Sci.*, **2012**, *258*, 8673–8677.

[23] Y. Kawamura, N. Hattori, N. Miyatake and Y. Uraoka, *J. Vac. Sci. Technol. Vac. Surf. Films*, **2013**, *31*, 01A142.

[24] P. Marchand and C. J. Carmalt, *Coord. Chem. Rev.*, **2013**, *257*, 3202–3221.

[25] T. Maruyama and J. Shionoya, *J. Mater. Sci. Lett.*, **1992**, *11*, 170–172.

[26] H. Sato, T. Minami, T. Miyata, S. Takata and M. Ishii, *Thin Solid Films*, **1994**, *246*, 65–70.

[27] J. Auld, D. J. Houlton, A. C. Jones, S. A. Rushworth, M. A. Malik, P. O'Brien and G. W. Critchlow, *J. Mater. Chem.*, **1994**, *4*, 1249.

[28] D. Pugh, P. Marchand, I. P. Parkin and C. J. Carmalt, *Inorg. Chem.*, **2012**, *51*, 6385–6395.

[29] J. S. Matthews, O. Just, B. Obi-Johnson and W. S. Rees, Jr., *Chem. Vap. Depos.*, **2000**, *6*, 129–132.

[30] S. Lim, B. Choi, Y. Min, D. Kim, I. Yoon, S. S. Lee and I.-M. Lee, *J. Organomet. Chem.*, **2004**, *689*, 224–237.
[31] J. S. Matthews, O. O. Onakoya, T. S. Ouattara and R. J. Butcher, *Dalton Trans.*, **2006**, 3806.
[32] J. Holmes, K. Johnson, B. Zhang, H. E. Katz and J. S. Matthews, *Appl. Organomet. Chem.*, **2012**, *26*, 267–272.
[33] D. Bekermann, D. Rogalla, H.-W. Becker, M. Winter, R. A. Fischer and A. Devi, *Eur. J. Inorg. Chem.*, **2010**, *2010*, 1366–1372.
[34] D. Bekermann, A. Ludwig, T. Toader, C. Maccato, D. Barreca, A. Gasparotto, C. Bock, A. D. Wieck, U. Kunze, E. Tondello, R. A. Fischer and A. Devi, *Chem. Vap. Depos.*, **2011**, *17*, 155–161.
[35] M. E. F. Braibante, H. S. Braibante, L. Missio and A. Andricopulo, *Synthesis*, **1994**, *1994*, 898–900.
[36] B. S. Kumar, A. Dhakshinamoorthy and K. Pitchumani, *Catal. Sci. Technol.*, **2014**, *4*, 2378.
[37] R. Romero, M. C. López, D. Leinen, F. Martín and J. R. Ramos-Barrado, *Mater. Sci. Eng. B*, **2004**, *110*, 87–93.
[38] B. S. Shaheen, H. G. Salem, M. A. El-Sayed and N. K. Allam, *J. Phys. Chem. C*, **2013**, *117*, 18502–18509.
[39] S. Kaleemulla, N. Madhusudhana Rao, M. Girish Joshi, A. Sivasankar Reddy, S. Uthanna and P. Sreedhara Reddy, *J. Alloys Compd.*, **2010**, ***504***, 351–356.
[40] J. Tauc, *Mater. Res. Bull.*, **1968**, *3*, 37–46.
[41] O. V. Dolomanov, L. J. Bourhis, R. J. Gildea, J. A. K. Howard and H. Puschmann, *J. Appl. Crystallogr.*, **2009**, *42*, 339–341.
[42] L. Palatinus and G. Chapuis, *J. Appl. Crystallogr.*, **2007**, *40*, 786–790.
[43] G. M. Sheldrick, *Acta Crystallogr. A*, **2008**, *64*, 112–122.
[44] L. J. Bourhis, O. V. Dolomanov, R. J. Gildea, J. A. K. Howard and H. Puschmann, *Acta Crystallogr. Sect. Found. Adv.*, **2015**, *71*, 59–75.

Table of Contents

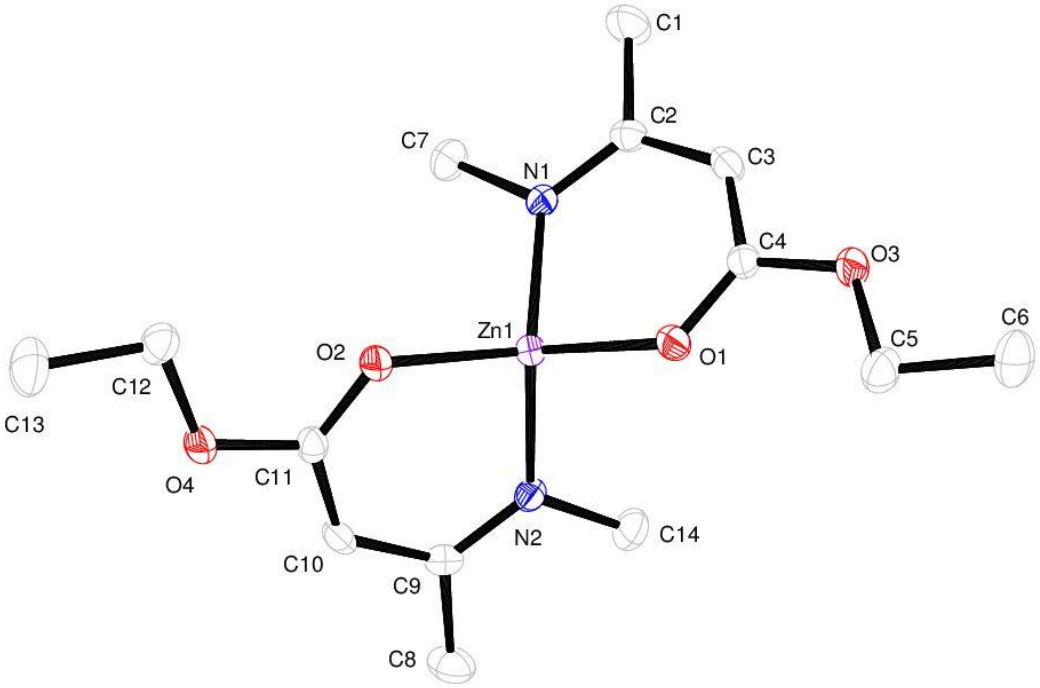

The synthesis, isolation and characterisation of zinc *β*-iminoesterate precursors of the type [Zn($CH_3C(NR)CHC(O)OCH_2CH_3$)] are described, as well as their use for the first time in the aerosol assisted chemical vapour deposition (AACVD) of ZnO thin films at 450 °C. Results show that changing the R group on the N moiety of the precursors has a significant effect on carbon contamination in the films.

Click here to download Graphical Material: Figure1.jpg

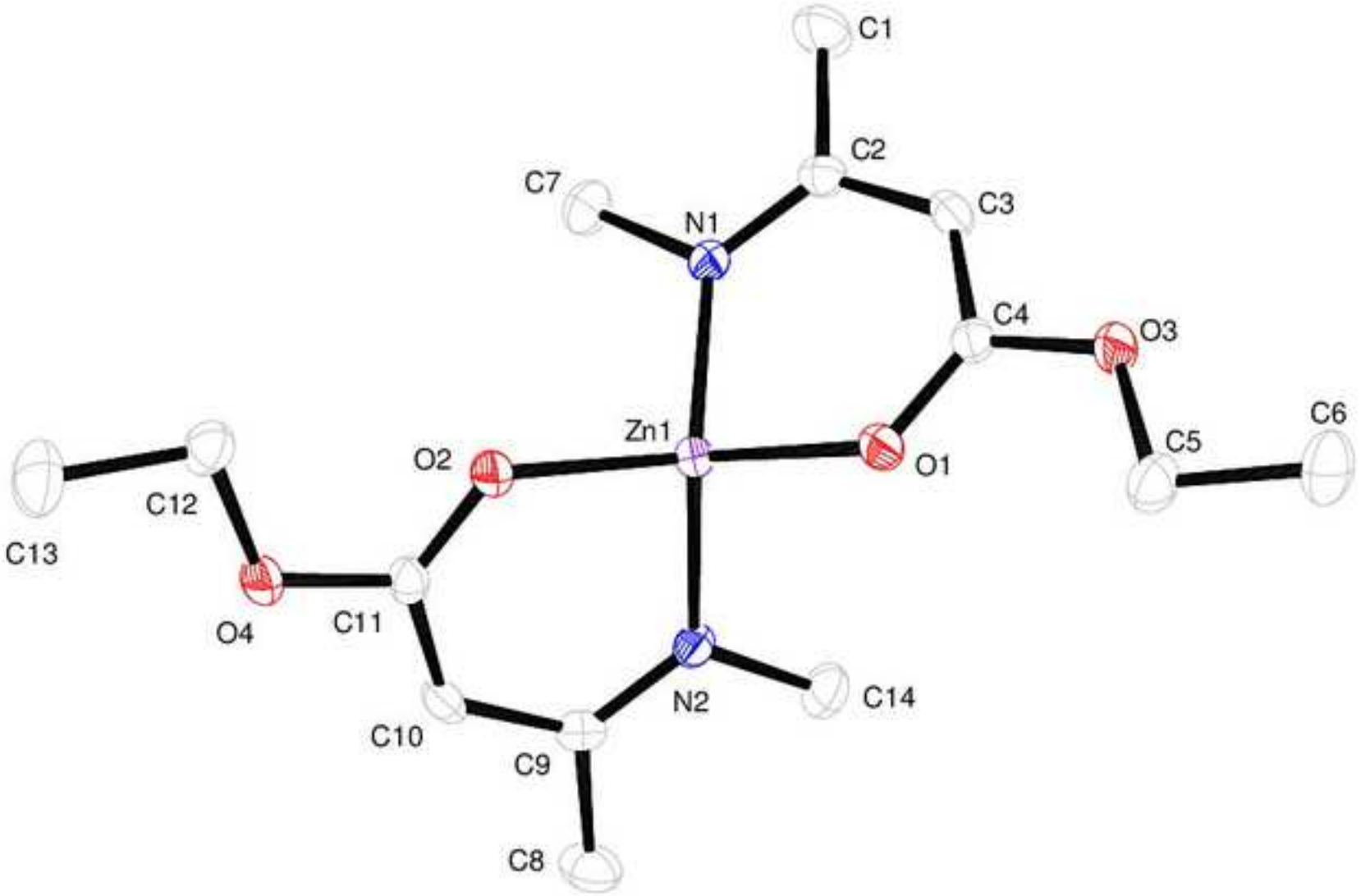

Click here to download Graphical Material: Figure2.tif

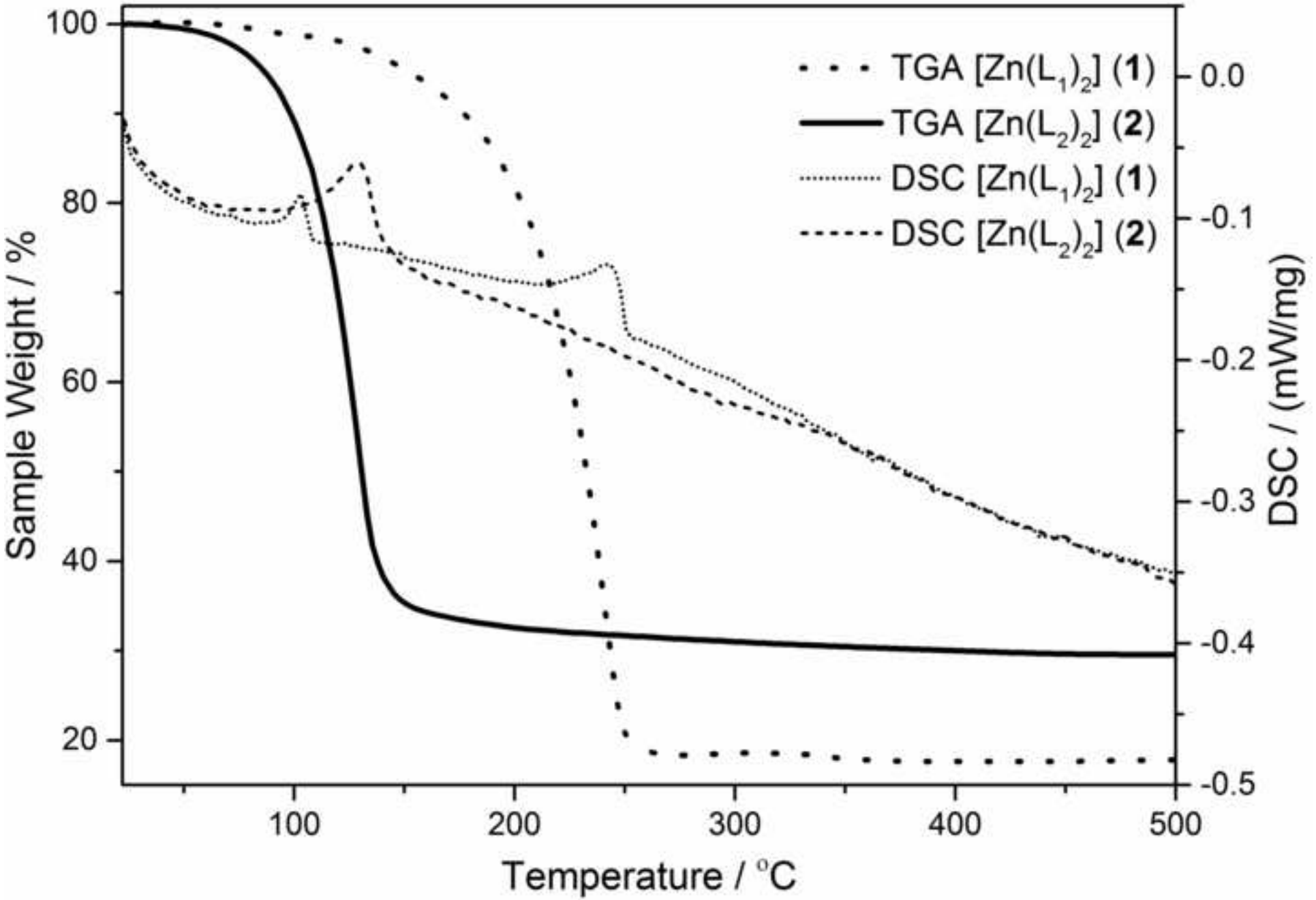

Click here to download Graphical Material: Figure3.tif

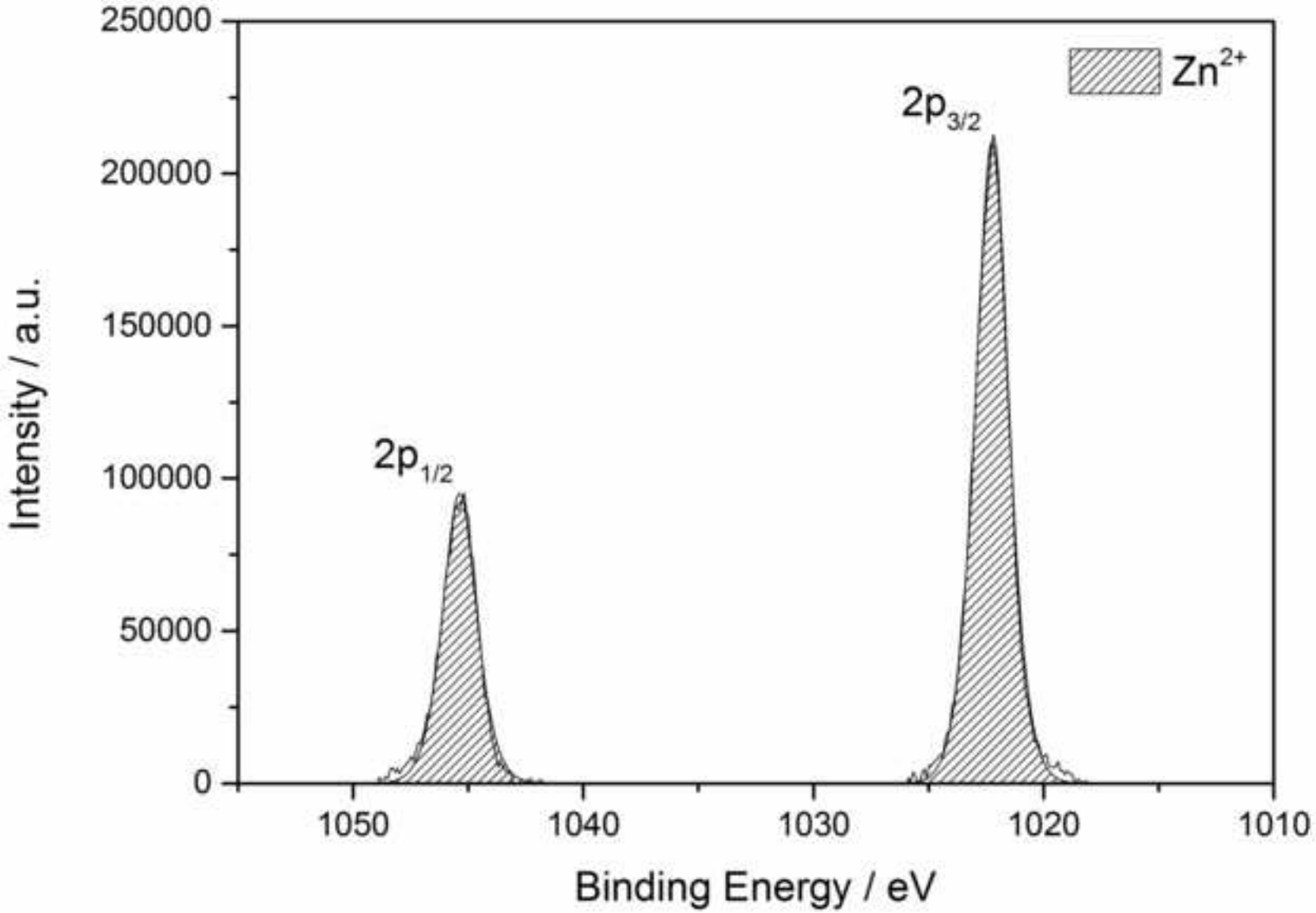

Click here to download Graphical Material: Figure4_Lower.tif

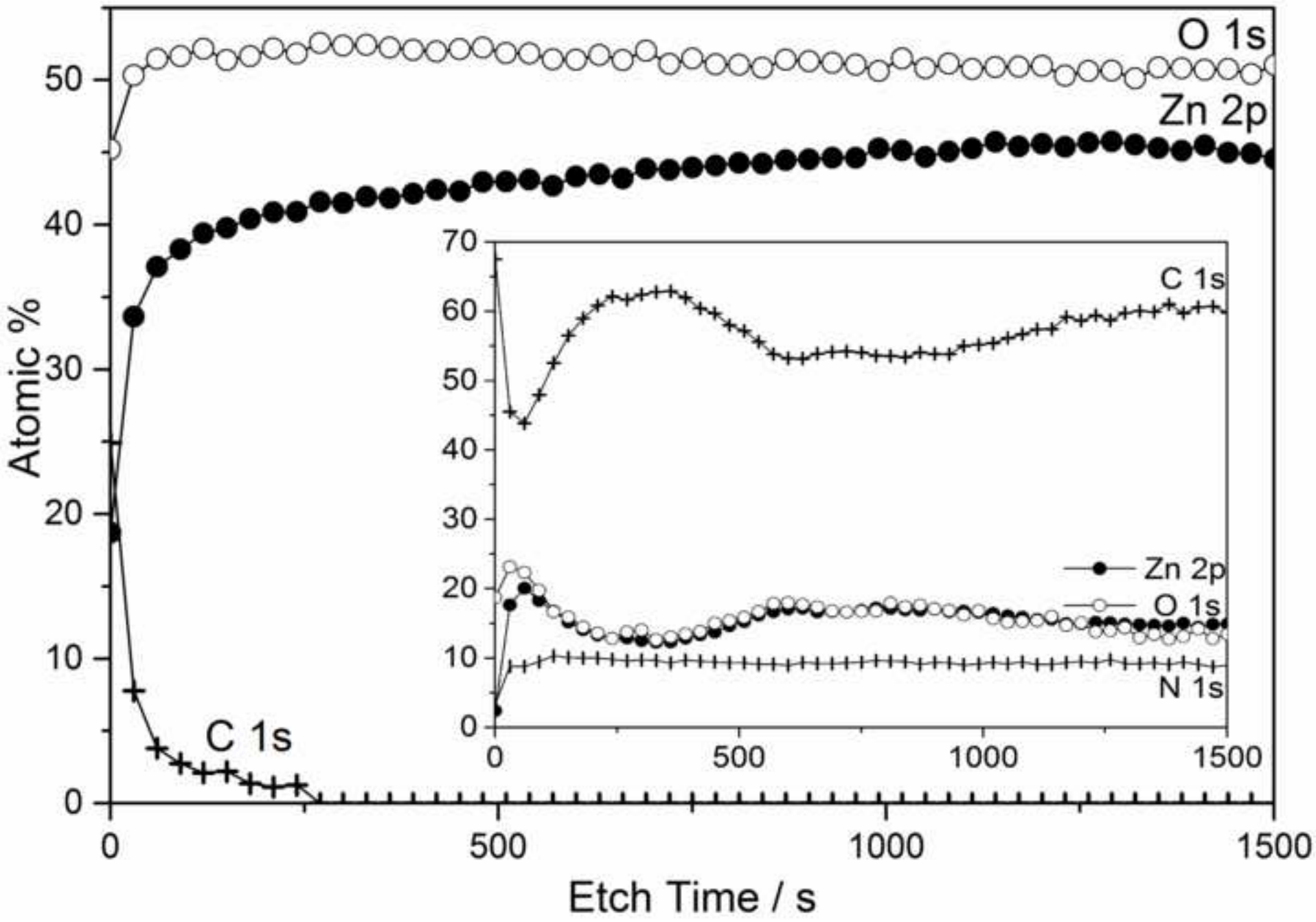

Click here to download Graphical Material: Figure4_Upper.tif

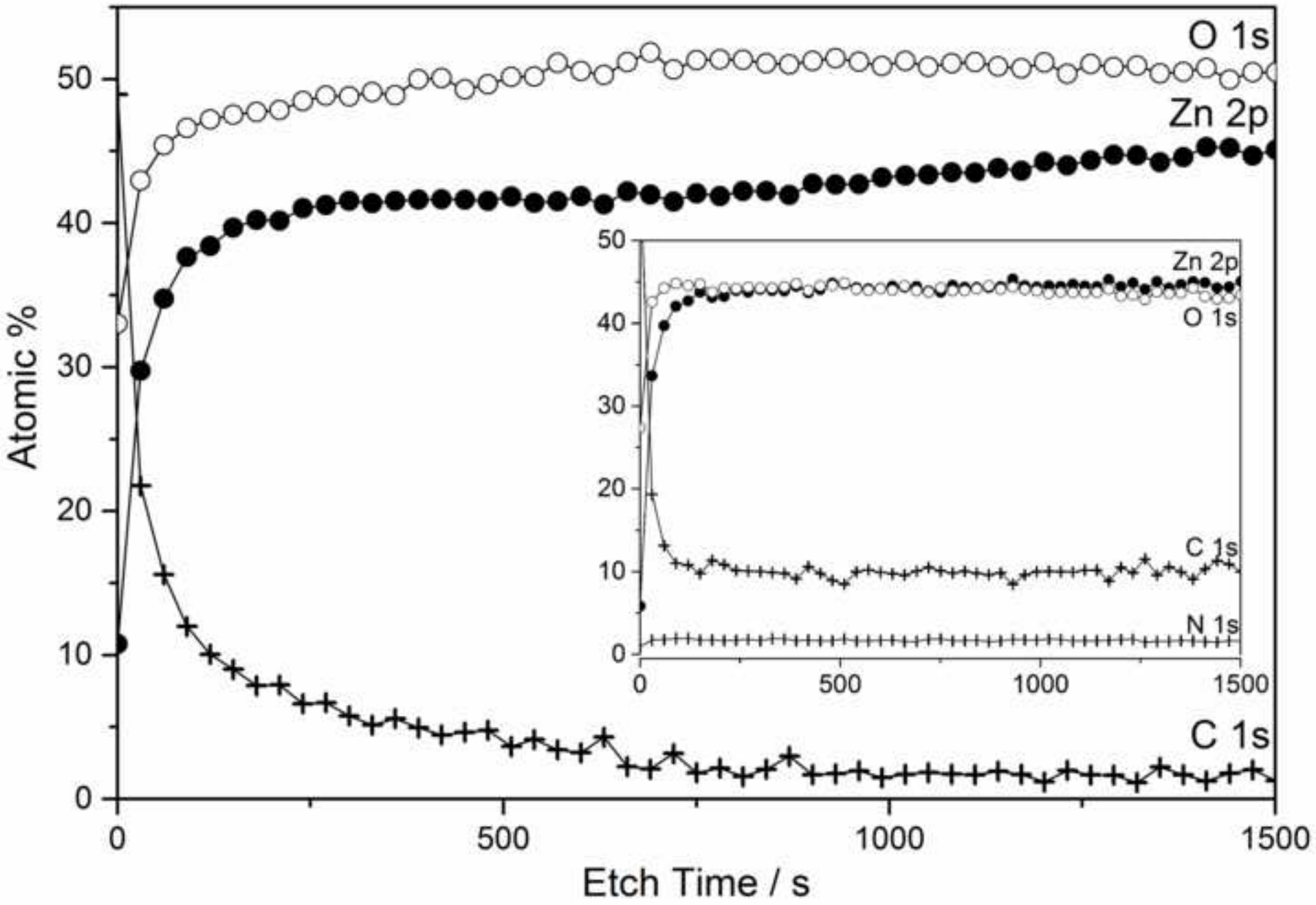

Click here to download Graphical Material: Figure5.tif

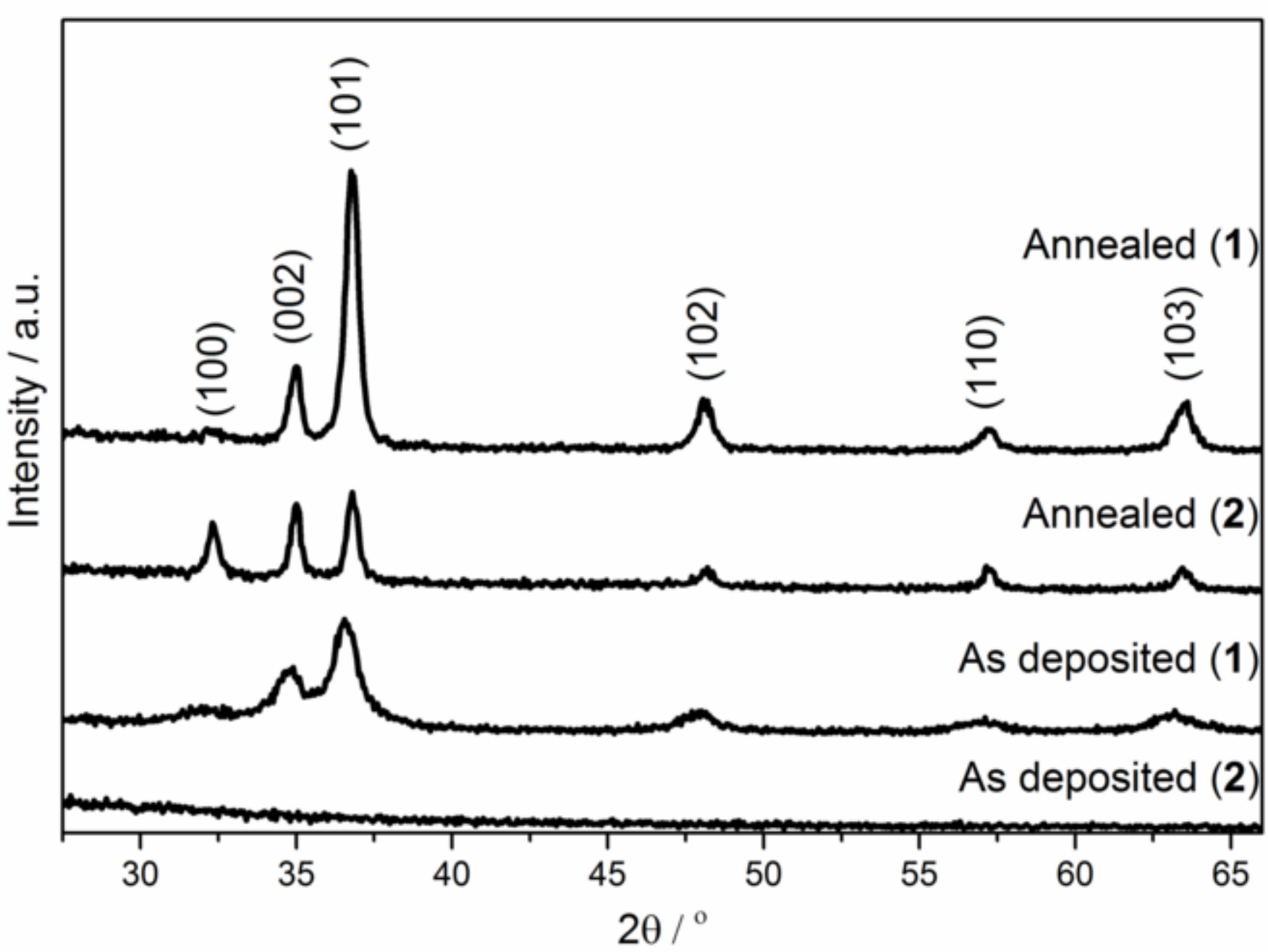

Click here to download Graphical Material: Figure6.docx

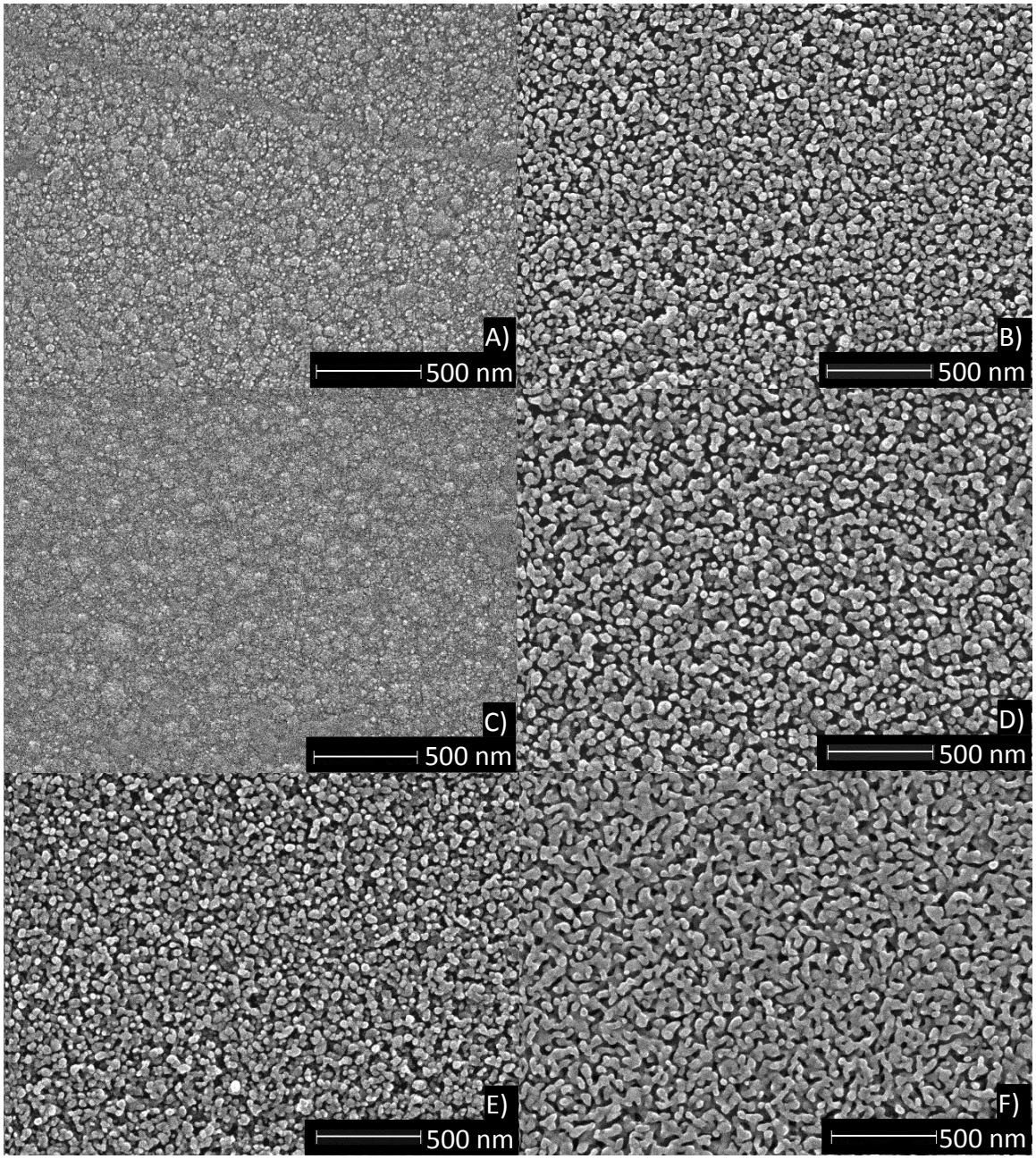

Click here to download Graphical Material: Figure7.tif

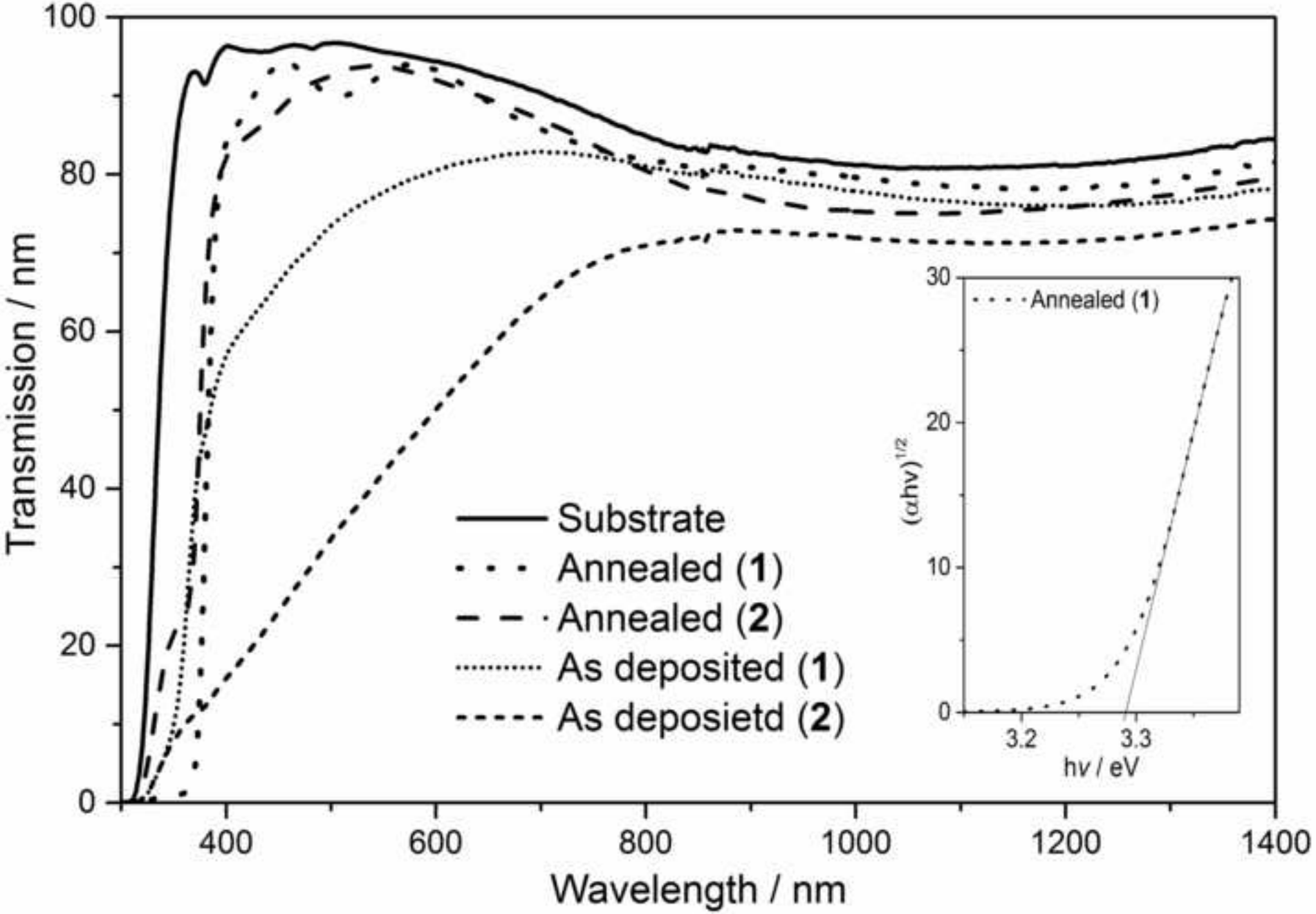

Supporting Information

Click here to download Supporting Information: Supplimentary Information.docx

Supporting Information - cif

Click here to download Supporting Information: XSTR0075.cif

Supporting Information - checkcif

Click here to download Supporting Information: XSTR0075_cifreport.pdf

Supporting Information - p4p file

Click here to download Supporting Information: XSTR0075.p4p